Uniform and nonuniform textures of a nematic liquid crystal in contact with an inhomogeneous substrate

S. Kondrat and A. Poniewierski
Institute of Physical Chemistry, Polish Academy of Sciences, Kasprzaka 44/52, 01-224 Warsaw, Poland
(Received 27 April 2001; published 29 August 2001)

A semi-infinite sample of a nematic liquid crystal in contact with a flat solid substrate, possessing an alternating stripe pattern of planar and homeotropic anchoring, is studied in the framework of the Frank-Oseen model. The case of strong anchoring on one of the stripes is treated by means of bifurcation analysis, whereas the case of weak anchoring is studied by means of numerical minimization of the free energy functional. We find a second order phase transition between the uniform homeotropic or planar alignment and a distorted director configuration. The effect of the stripe width and the anchoring strength on the location of this transition and on the bulk orientation of the nematic director is also studied.

DOI: 10.1103/PhysRevE.64.031709 PACS number(s): 64.70.Md, 61.30.Cz

I. INTRODUCTION

Nematic liquid crystals are anisotropic fluids exhibiting a long range orientational order of uniaxial symmetry, with the local symmetry axis defined by a unit vector $\hat{\mathbf{n}}$ called the director. It is well known that the surface of a solid substrate, as well as other limiting surfaces, have the ability to orient $\hat{\mathbf{n}}$ along a well defined direction called the easy axis [1]. On the phenomenological level the easy axis is defined as the orientation of $\hat{\mathbf{n}}$ preferred by the liquid-crystal–substrate interactions, i.e., that minimizing the surface free energy F_s in the absence of bulk distortions or external fields. This substrate induced alignment of liquid crystals, known as anchoring [1,2], has important practical applications. To achieve the desired director orientation and anchoring strength various substrates and surface treatments are used [2–7].

In many model studies of liquid-cystal–substrate interfaces the details of surface structure at the nanometer scale are neglected and the substrate surface is treated as homogeneous [8–12]. On the other hand, a long time ago Berreman [13] showed that due to the elastic strain energy anisotropic surface roughness can induce a molecular orientation parallel to the direction of grooves produced by rubbing the substrate surface. To obtain the azimuthal anchoring energy he assumed a sinusoidal shape of the surface, with wavelength ~ 200 Å and amplitude ~ 10 Å, and the director locally parallel to the surface, i.e., strong polar anchoring. The latter assumption was generalized by Faetti [14], who took into account a finite value of the polar anchoring energy. Another type of nonuniform surface was considered by Barbero *et al.* [15]. In their work, the surface roughness is not considered explicitly; nevertheless, the spatial distribution of easy directions is taken into account. This is achieved by assuming that the surface has a periodic structure with two stripes characterized by different easy directions and, in general, different widths. In addition, $\hat{\mathbf{n}}$ is constrained to stay in the plane normal to the stripes, and in the case of weak anchoring the quadratic approximation for the anchoring energy is applied. The latter assumption implies that the easy directions should not differ too much from each other. Thus, this model is used to study the effective easy direction induced by the periodic substrate as well as the effective surface energy.

In more recent work, Qian and Sheng [16,17] also applied the idea of a periodic substrate to an alternating stripe pattern of random planar and homeotropic substrate potentials, with periodicity in the mesoscopic range, i.e., ~ 0.5 μm or less. While the prior studies of inhomogeneous substrates considered the elastic energy only in the Frank-Oseen form, Qian and Sheng apply the Landau–de Gennes formalism [1], where the tensor nematic order parameter $\mathbf{Q}$ is used instead of $\hat{\mathbf{n}}$. Assuming stripes of equal width they found two stable states of the bulk director: the yz state, with $\hat{\mathbf{n}}$ in the plane normal to the surface and parallel to the stripes, and the x state, with $\hat{\mathbf{n}}$ parallel to the surface and normal to the stripes. A first order phase transition between these two states can be induced either by changing the temperature or by changing the periodicity of the structure. It is argued that the transition occurs when the elastic energy becomes unfavorably large compared to the surface alignment potential, and this is observed for decreasing periodicity. This study shows that despite the azimuthal degeneracy in each stripe the whole structure does align the liquid crystal in a well defined azimuthal direction. Indeed, in a very recent experimental work, Lee and Clark [18] have demonstrated that molecular-scale anisotropy or roughness is not required to achieve liquid crystal alignment. They showed that the alignment can be induced by a surface lithographically divided into two distinct molecularly smooth isotropic regions. Thus, it is governed only by the pattern of boundary lines between the isotropic regions and by the liquid crystal elasticity. The simplest pattern studied experimentally in [18] consisted of homeotropic and random planar stripes of total width in the range of 10 μm.

In this paper, we apply the model introduced by Barbero *et al.* in [15] to the specific case of mixed homeotropic and planar anchoring, where the latter is in the direction normal to the stripes. With this choice of anchoring direction it is possible that despite the periodic surface structure the adjacent nematic liquid crystal will remain uniform. This possibility was not considered in [15], however. Therefore, we study in detail the relation between the width and the anchoring strength of the stripes and the director configuration in the surface region and in the bulk. In particular, we find the stability limits of the homeotropic and planar textures in terms of the model parameters. To obtain the phase diagram

 ©2001 The American Physical Society

we apply the Frank-Oseen formalism and the Rapini-Papoular [19] form of the anchoring energy. We also consider the limit of strong anchoring on one of the stripes and the competition between the alignments induced by the weak anchoring and strong anchoring stripes when the width of the latter tends to zero.

Our paper is organized as follows. In Sec. II, we recall the model introduced in [15]. The case of strong anchoring on one of the stripes is studied in Sec. III by means of a bifurcation analysis. In Sec. IV weak anchoring on both stripes is assumed. To study this case we first derive the free energy of the system as a functional of the surface director alone. Minimization of an approximate form of this functional leads to a Schrödinger type differential equation, which can be easily solved (Sec. IV A). The results of the exact numerical minimization of the free energy are presented in Sec. IV B. Finally, Sec. V is devoted to the conclusions.

II. THE MODEL

We consider a flat substrate whose surface is physically or chemically inhomogeneous. This inhomogeneity is characterized by a periodic stripe pattern of wavelength p along the x direction; the z axis is perpendicular to the surface, and the y axis is parallel to the stripes. We assume homeotropic anchoring on the stripe $0 \leqslant x < p_1$, where p_1 is its width, and planar homogeneous anchoring along the x direction on the stripe $p_1 \leqslant x < p$. Due to the translational invariance in the y direction $\hat{\mathbf{n}}$ depends only on x and z. We also restrict ourselves to the case when $\hat{\mathbf{n}}$ is everywhere parallel to the xz plane, i.e., $\hat{\mathbf{n}} = \hat{\mathbf{x}} \sin\theta + \hat{\mathbf{z}} \cos\theta$ (no twist deformation). Assuming that the bend and splay elastic constants are equal ($K_1 = K_3 = K$), which is not far from experimental data (see, e.g., [20,21]) and is consistent with the Landau–de Gennes theory, we obtain the distortion free energy per unit length and per period,

$$F_d = \frac{K}{2} \int_0^p dx \int_0^\infty dz (\boldsymbol{\nabla} \theta)^2. \tag{2.1}$$

For the surface free energy we use the Rapini-Papoular expression [19]

$$F_s = \frac{1}{2} \int_0^p dx w(x) \sin^2 \theta_0(x), \tag{2.2}$$

where $\theta_0(x) = \theta(x, z=0)$, and $w(x)$ is the anchoring strength. In the homeotropic region ($0 \leqslant x < p_1$) $w(x) = w_1$, whereas in the planar region ($p_1 \leqslant x < p$) $w(x) = -w_2$, with $w_1, w_2 \geqslant 0$. Thus the total free energy per period as a functional of $\theta(x,z)$ assumes the following form:

$$F = \frac{K}{2} \int_0^p dx \int_0^\infty dz (\boldsymbol{\nabla} \theta)^2 + \frac{w_1}{2} \int_0^{p_1} dx \sin^2 \theta_0(x) - \frac{w_2}{2} \int_{p_1}^p dx \sin^2 \theta_0(x). \tag{2.3}$$

Minimization of F leads to the Laplace equation

$$\nabla^2 \theta(x,z) = 0 \tag{2.4}$$

with the boundary conditions

$$\begin{aligned} K(\partial\theta/\partial z)\big|_{z=0} &= w_1 \theta_0(x) \quad \text{for } 0 \leqslant x < p_1, \\ K(\partial\theta/\partial z)\big|_{z=0} &= -w_2 \theta_0(x) \quad \text{for } p_1 \leqslant x < p. \end{aligned} \tag{2.5}$$

III. STRONG ANCHORING LIMIT

When the nematic-nematic V_{nn} and the nematic-substrate V_{ns} interactions are of the same order then the extrapolation length $b = K/w \sim a V_{nn}/V_{ns} \sim a$, where a denotes a molecular dimension. Then, in the continuum limit, it is justified to put $b = 0$ and assume that the director orientation at the surface is fixed [1]. This is known as the strong anchoring limit. Let us assume that the strong anchoring occurs on one of the stripes, and we take it to be the stripe with homeotropic anchoring. This means that the extrapolation length $b_1 = K/w_1 = 0$ and $\theta_0(x) = 0$, for $0 \leqslant x < p_1$. The planar anchoring on the stripe $p_1 \leqslant x < p$ is assumed to be weak, i.e., $b_2 = K/w_2 \neq 0$.

It is rather obvious that for small w_2 the strong homeotropic anchoring prevails and $\theta(x,z) = 0$ everywhere. However, the decrease of the width p_1 or the increase of w_2 should effectively weaken the effect of strong anchoring and eventually would result in a nonuniform director configuration. To investigate the loss of stability of the uniform $\theta_0(x,z) = 0$ state the free energy in Eq. (2.3) is approximated by

$$F = \frac{K}{2} \int_0^p dx \int_0^\infty dz [\boldsymbol{\nabla} \theta(x,z)]^2 - \frac{w_2}{2} \int_{p_1}^p dx [\theta_0(x)]^2, \tag{3.1}$$

which means that small θ_0 is assumed. Now we seek a periodic solution of the Laplace equation (2.4) satisfying the boundary condition $\theta_0(x) = 0$, for $0 \leqslant x < p_1$. A general periodic solution of the Laplace equation has the form of the Fourier expansion

$$\theta(x,z) = \sum_{n=0}^\infty [\theta_n^{(s)} \sin(knx) + \theta_n^{(c)} \cos(knx)] e^{-nkz}, \tag{3.2}$$

where $k = 2\pi/p$, and $\theta_n^{(s)}$ and $\theta_n^{(c)}$ are to be determined from the boundary condition. The distortion part of the free energy takes the following simple form:

$$F_d = \frac{\pi K}{2} \sum_{n=1}^\infty n[(\theta_n^{(s)})^2 + (\theta_n^{(c)})^2]. \tag{3.3}$$

In general, $\theta_0(x)$ satisfying the boundary condition for $0 \leqslant x < p_1$ and continuous at $x = p_1$ and $x = p$ is given by

$$\theta_0(x) = \Theta(x - p_1) f(x), \tag{3.4}$$

where $\Theta(x)$ is the Heaviside step function and $f(x)$ is an arbitrary function satisfying the continuity condition $f(p_1) = f(p) = 0$. Therefore, it can be expressed as follows:

$$f(x)=\sum_{n=1}^{\infty} B_n \sin[k' n(x-p_1)], \tag{3.5}$$

where $k'=\pi/p_2$ and $p_2=p-p_1$. To study the stability of the $\theta(x,z)=0$ solution we express F in terms of the amplitudes B_n. For the surface part we have

$$F_s=-\frac{p_2 w_2}{4}\sum_{n=1}^{\infty} B_n^2, \tag{3.6}$$

and to obtain F_d we first find $\theta_n^{(s)}$ and $\theta_n^{(c)}$ from Eqs. (3.2), (3.3), and (3.5), which for $n>0$ gives

$$\theta_n^{(s)}=\frac{2}{p}\int_0^p \theta_0(x)\sin(nkx)dx$$

$$=\frac{p}{2\pi p_2}\sum_{n'} B_{n'}\frac{n'\sin(2\pi n p_1/p)}{(n'p/2p_2)^2-n^2}, \tag{3.7}$$

$$\theta_n^{(c)}=\frac{2}{p}\int_0^p \theta_0(x)\cos(nkx)dx$$

$$=\frac{p}{2\pi p_2}\sum_{n'} B_{n'}\frac{n'[\cos(2\pi n p_1/p)-(-1)^{n'}]}{(n'p/2p_2)^2-n^2}. \tag{3.8}$$

Finally, we obtain for the free energy

$$F=\frac{K}{4}\sum_{n'=1}^{\infty}\sum_{n''=1}^{\infty}\left\{n'n''\Psi_{n'n''}-\frac{p_2}{b_2}\delta_{n'n''}\right\}B_{n'}B_{n''}, \tag{3.9}$$

where δ_{nm} is the Kronecker delta symbol, and

$$\Psi_{n'n''}=\frac{p^2}{2\pi p_2^2}\sum_{n=1}^{\infty}\frac{n\{1+(-1)^{n'+n''}-[(-1)^{n'}+(-1)^{n''}]\cos(2\pi n p_1/p)\}}{[(n'p/2p_2)^2-n^2][(n''p/2p_2)^2-n^2]}. \tag{3.10}$$

When the quadratic form (3.9) is positive definite the uniform solution $\theta=0$ is stable. At fixed p_1/p_2, the loss of stability of the $\theta=0$ solution occurs when the ratio p_2/b_2 becomes equal to the smallest eigenvalue of the matrix $\Psi_{n'n''}$. Truncation of the Fourier expansion (3.5) after the first term results in the following condition for the stability limit:

$$\frac{p_2}{b_2}=\Psi_{11}(p_1/p_2)=\frac{(1+p_1/p_2)^2}{\pi}\psi(p_1/p_2), \tag{3.11}$$

where

$$\psi(x)=\sum_{n=1}^{\infty} n\frac{1+\cos[2\pi n x/(1+x)]}{[(1+x)^2/4-n^2]^2}. \tag{3.12}$$

From this simple approximation we obtain the qualitatively correct shape of the bifurcation line, which is shown in Fig. 1. However, the rigorous procedure requires diagonalization of the quadratic form (3.9). We have performed numerical diagonalization, truncating the Fourier expansion of $f(x)$ at $n=N$, for various values of N, and the bifurcation lines obtained in this way are presented in Fig. 1. In Fig. 2, we plot p_2/b_2 against N for selected points on the bifurcation line. It is clear that the large N asymptotic behavior of p_2/b_2 depends on the ratio p_1/p_2. We observe that for $p_1/p_2\neq 0$ the ratio p_2/b_2 tends to a nonzero limit when $N\to\infty$. However, the case $p_1/p_2=0$ is different as then p_2/b_2 seems to tend to zero, albeit very slowly. Since the limit $N\to\infty$ should be performed first this behavior suggests that p_2/b_2 as a function of p_1/p_2 is discontinuous at $p_1/p_2=0$, i.e., it has a nonzero limit when $p_1/p_2\to 0$ but vanishes when $p_1=0$. Of course, the matrix $\Psi_{n'n''}$ is by definition positive definite [see Eq. (3.3)] and $F_d=0$ only if $\theta_0=$const, for $0<x<p$, which is incompatible with the boundary conditions at $x=0$ and $x=p$, however. On the other hand, a constant profile can result from the Fourier expansion (3.5) when the number of Fourier components tends to infinity. This explains why the smallest eigenvalue of $\Psi_{n'n''}$ vanishes for $p_1=0$. When

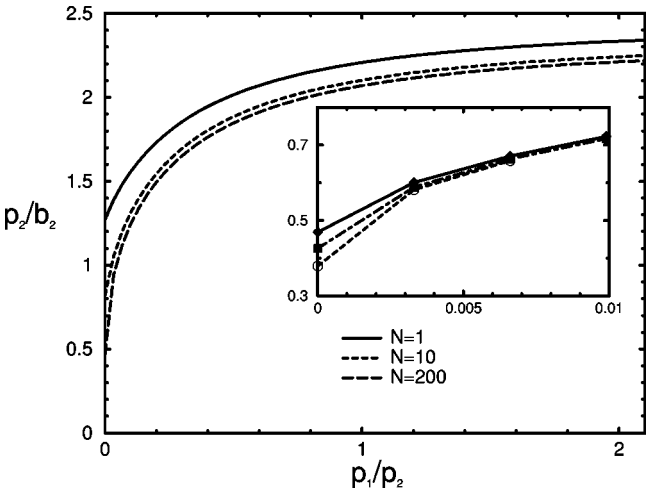

FIG. 1. Bifurcation line showing the stability limit of the uniform homeotropic texture in the case of strong anchoring on the homeotropic stripe, obtained for different numbers N of Fourier components in the expansion of a nonuniform surface perturbation [see Eq. (3.5)]. The inset shows the region of small p_1/p_2 for $N=200$ (diamonds), $N=500$ (squares), and $N=1000$ (circles).

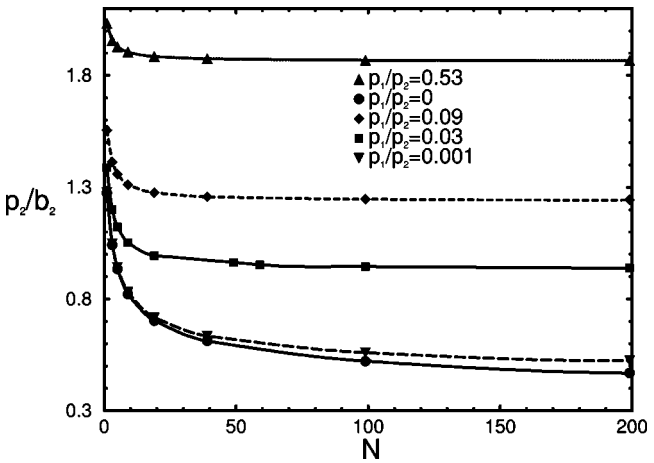

FIG. 2. Bifurcation value of p_2/b_2 as a function of the number of Fourier components, for a few values of the ratio p_1/p_2.

$p_1 \neq 0$ the above argumentation does not hold, however, because F_d in Eq. (3.3) diverges if $\theta_0 = \text{const}$ for $p_1 < x < p$.

IV. WEAK ANCHORING

In this section, we assume that anchoring on both the planar and the homeotropic stripes is of finite strength, which is usually referred to as weak anchoring. Now the substrate is characterized by two nonzero extrapolation lengths $b_1 = K/w_1$ and $b_2 = K/w_2$, and the free energy of the system is given by Eq. (2.3). In the absence of the distortion term in Eq. (2.3) there would be only homogeneous states $\theta(x,z) = 0$ and $\theta(x,z) = \pi/2$, and the transition between them would occur when

$$\frac{b_1}{b_2} = \frac{p_1}{p_2}. \tag{4.1}$$

To take into account distortions we proceed as follows. First, we minimize F_d with respect to all functions $\theta(x,z)$ that satisfy the boundary condition $\theta(x,z=0) = \theta_0(x)$, where $\theta_0(x)$ is an arbitrary continuous and periodic (with the period p) function of x. This minimization results in the Laplace equation $\nabla^2\theta = 0$; thus, F_d can be transformed to

$$\begin{aligned} 2F_d/K &= \int_0^p dx \int_0^\infty dz (\nabla\theta)^2 \\ &= \int_0^p dx \int_0^\infty dz [\nabla(\theta\nabla\theta) - \nabla^2\theta] \\ &= -\lim_{z\to 0} \int_0^p dx\, \theta \frac{\partial\theta}{\partial z}, \end{aligned} \tag{4.2}$$

where we have used the periodicity of θ and the bulk condition $\theta \to \text{const}$ for $z \to \infty$. Now F_d can be explicitly expressed as a functional of $\theta_0(x)$. To show this we present $\theta(x,z)$ as a convolution

$$\theta(x,z) = \frac{1}{p}\int_0^p dx'\, \theta_0(x') g(x'-x,z), \tag{4.3}$$

where the propagator $g(x,z)$ satisfies the Laplace equation with the boundary condition

$$\lim_{z\to 0} g(x,z) = p\,\delta(x), \tag{4.4}$$

where $\delta(x)$ is the Dirac δ function. It is straightforward to show that

$$g(x,z) = \sum_{n=-\infty}^{\infty} \exp(-|n|kz + inkx) \tag{4.5}$$

with $k = 2\pi/p$. Note also that because $g(x,z) \to 1$ when $z \to \infty$ the bulk value of θ can be expressed from Eq. (4.3) in terms of θ_0 as follows:

$$\theta_b = \frac{1}{p}\int_0^p dx\, \theta_0(x). \tag{4.6}$$

For convenience we define a complex function

$$G(\zeta) = \sum_{n=1}^{\infty} e^{-kn\zeta} = \frac{e^{-k\zeta}}{1-e^{-k\zeta}}; \tag{4.7}$$

hence,

$$g(x,z) = 1 + G(z+ix) + G(z-ix) = 1 + G^+(x,z), \tag{4.8}$$

where

$$G^+(x,z) = \frac{\cos(kx) - e^{-kz}}{\cosh(kz) - \cos(kx)}. \tag{4.9}$$

Substituting Eqs. (4.3) and (4.8) into Eq. (4.2) and replacing $\partial G(z \pm ix')/\partial z$ by $\mp i \partial G(z \pm ix')/\partial x'$ we obtain

$$\begin{aligned} 2F_d/K &= -\frac{i}{p}\lim_{z\to 0}\int_0^p dx \int_0^p dx'\, \theta_0(x)\theta_0(x') \frac{\partial}{\partial x'} G^-(x-x',z) \\ &= \frac{i}{2p}\lim_{z\to 0}\int_0^p dx \int_0^p dx' [\theta_0(x) - \theta_0(x')]^2 \frac{\partial}{\partial x'} \\ &\quad \times G^-(x-x',z), \end{aligned} \tag{4.10}$$

where

$$G^-(x,z) = G(z+ix) - G(z-ix) = \frac{-i\sin(kx)}{\cosh(kz) - \cos(kx)}, \tag{4.11}$$

and we have used the fact that the integrals of $\theta_0^2(x)\partial G^-/\partial x'$ and $\theta_0^2(x')\partial G^-/\partial x'$ vanish because of the periodic boundary conditions in the x direction. Finally, we perform the limit $z \to 0$ in Eq. (4.10) and obtain the following simple expression for the distortion free energy:

$$F_d=\frac{\pi K}{4p^2}\int_0^p dx\int_0^p dx'\frac{[\theta_0(x)-\theta_0(x')]^2}{\sin^2[\pi(x-x')/p]}. \quad (4.12)$$

In what follows we use dimensionless quantities: $\tilde{F}=F/K$, $\tilde{b}_i=b_i/p$ $(i=1,2)$, and $r_1=p_1/p$. Thus, the total free energy as a functional of θ_0 is given by

$$\tilde{F}=\frac{\pi}{4}\int_0^1 dx\int_0^1 dx'\frac{[\theta_0(x)-\theta_0(x')]^2}{\sin^2[\pi(x-x')]}+\frac{1}{2\tilde{b}_1}\int_0^{r_1}\sin^2\theta_0(x)dx$$

$$-\frac{1}{2\tilde{b}_2}\int_{r_1}^1\sin^2\theta_0(x)dx, \quad (4.13)$$

where now x and x' are measured in units of p.

To find the equilibrium $\theta_0(x)$ one can minimize $\tilde{F}$ and then solve the resulting nonlinear integral equation. Alternatively, one can minimize $\tilde{F}$ directly by means of numerical methods. In Sec. IV B we take the latter route; first, however, we study the problem using a simple approximation to the functional $\tilde{F}[\theta_0]$.

A. Square gradient approximation

It is instructive to consider first a simple approximation that results in a soluble equation for $\theta_0(x)$. Here we restrict ourselves to small θ_0 when $\sin\theta_0\approx\theta_0$. Moreover, we make use of the fact that the main contribution to the distortion free energy in Eq. (4.13) comes from the region $x\approx x'$, where $[\theta_0(x')-\theta_0(x)]/\sin[\pi(x'-x)]\approx(1/\pi)d\theta_0(x)/dx$. This approximation results in a simple square gradient form of $\tilde{F}$:

$$\tilde{F}=\frac{1}{2}\int_0^1\left[\frac{1}{2\pi}\left(\frac{d\theta_0}{dx}\right)^2+V(x)\theta_0^2(x)\right]dx, \quad (4.14)$$

and the Euler-Lagrange equation is of the Schrödinger equation type,

$$\frac{1}{2\pi}\frac{d^2\theta_0}{dx^2}-V(x)\theta_0(x)=0, \quad (4.15)$$

with the potential of a well,

$$V(x)=\begin{cases}1/\tilde{b}_1, & 0\leqslant x<r_1\\ -1/\tilde{b}_2, & r_1\leqslant x<1.\end{cases} \quad (4.16)$$

The general solution of Eq. (4.15) is

$$\theta_0(x)=A_1e^{k_1x}+B_1e^{-k_1x} \quad \text{for } 0\leqslant x<r_1$$

$$\theta_0(x)=A_2\sin(k_2x)+B_2\cos(k_2x) \quad \text{for } r_1\leqslant x<1, \quad (4.17)$$

where $k_i=\sqrt{2\pi/\tilde{b}_i}$, for $i=1,2$. To determine the four coefficients in Eq. (4.17) we use the condition that both θ_0 and $d\theta_0/dx$ are periodic and continuous founctions, which leads to a set of four linear equations for A_i and B_i. A nonzero solution exists only if the matrix of the equation is singular; otherwise only the $\theta_0=0$ solution is possible. The appearance of a nonzero solution of Eq. (4.17) means the loss of stability of the uniform solution. After some algebra we find that it occurs when the following relation between the parameters $\tilde{b}_1$, $\tilde{b}_2$, and r_1 holds:

$$\sqrt{\tilde{b}_1/\tilde{b}_2}=\frac{\{\cos[k_2(1-r_1)]\pm 1\}\{\cosh(k_1r_1)\mp 1\}}{\sin[k_2(1-r_1)]\sinh(k_1r_1)}. \quad (4.18)$$

First, let us consider relation (4.18) in the asymptotic limits of large or small $\tilde{b}_1$. In the limit of $\tilde{b}_1\to\infty$ we find

$$\frac{1}{\tilde{b}_2}\sim\frac{r_1}{1-r_1}\frac{1}{\tilde{b}_1}-\frac{\pi r_1^2}{1-r_1}\left(\frac{1}{2}-\frac{r_1}{6}\right)\left(\frac{1}{\tilde{b}_1}\right)^2, \quad (4.19)$$

which reduces to relation (4.1) when the second order term in $\tilde{b}_1^{-1}$, describing the effect of distortions in $\tilde{F}$, is neglected. In the opposite limit of strong anchoring $(\tilde{b}_1\to 0)$ we find

$$\frac{1}{\tilde{b}_2}\sim\frac{\pi}{2}(1-r_1)^{-2}, \quad (4.20)$$

which means that $\tilde{b}_2^{-1}$ saturates at large values of $\tilde{b}_1^{-1}$. The bifurcation value of $\tilde{b}_2^{-1}$ for an arbitrary value of $\tilde{b}_1^{-1}$ and at constant r_1 can be determined numerically. In the next subsection, we compare the square gradient approximation with the results of numerical minimization of $\tilde{F}$ given by Eq. (4.13).

B. Numerical minimization of the free energy

To minimize numerically the free energy functional given by Eq. (4.13) we first express it in a discrete form by defining $\theta_0(x)$ on a mesh $x_n=nh$, where $n=0,\ldots,N$ and $h=1/N$. Thus, $\tilde{F}$ becomes a function of variables $\theta_0^n=\theta_0(x_n)$, and because of the periodic boundary condition $\theta_0^N=\theta_0^0$ the number of independent variables is N. The distortion term in Eq. (4.13) assumes the following discrete form:

$$\tilde{F}_d=\frac{\pi}{4}\left\{h^2\sum_{n=0}^{N-1}\sum_{n\neq n'=0}^{N-1}\frac{(\theta_0^n-\theta_0^{n'})^2}{\sin^2[\pi h(n-n')]}+\frac{1}{\pi^2}\sum_{n=0}^{N-1}(\theta_0^{n+1}-\theta_0^n)^2\right\}, \quad (4.21)$$

where the second term corresponds to integration over the region $x\approx x'$, in which the integrand can be approximated by $\pi^{-2}(d\theta_0/dx)^2$. Then, we minimized $\tilde{F}(\theta_0^0,\ldots,\theta_0^{N-1})$ using the conjugate gradient algorithm [22]. Most of the calculations were performed with $N=200$ but in selected cases we have verified the results using $N=500$.

The main results of our numerical calculations are presented in Figs. 3–7. In Fig. 3, we show the phase diagram in

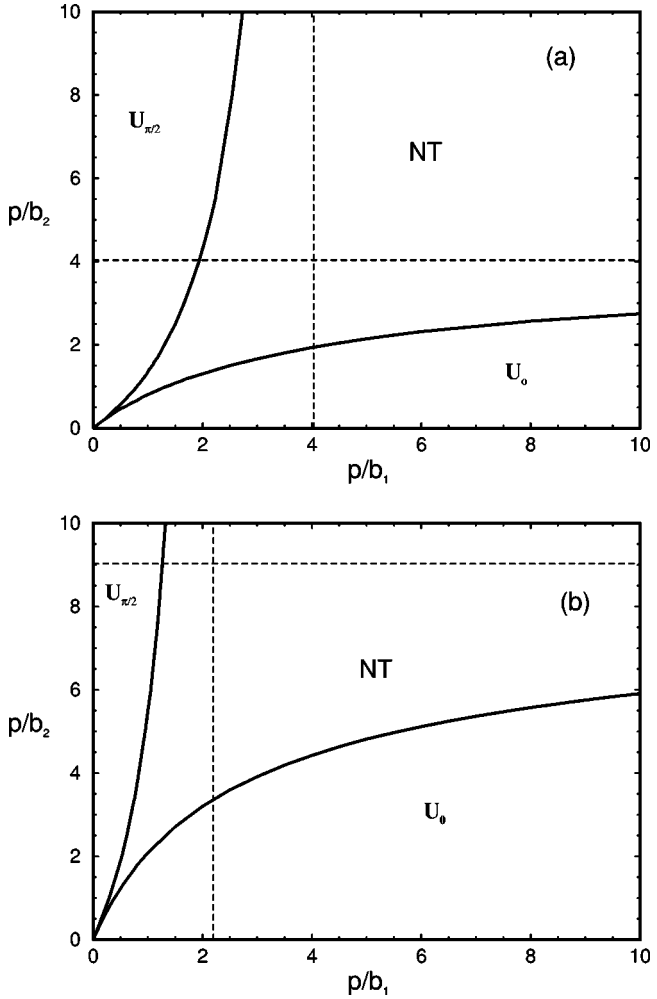

FIG. 3. Phase diagram obtained from the numerical minimization of the free energy functional, for two values of the stripe width ratio: (a) $p_1/p_2=1$ and (b) $p_1/p_2=3$. U_0, $U_{\pi/2}$, and NT denote the uniform homeotropic, the uniform planar, and the nonuniform textures, respectively. In the limit of strong anchoring, the transition lines approach the dashed lines.

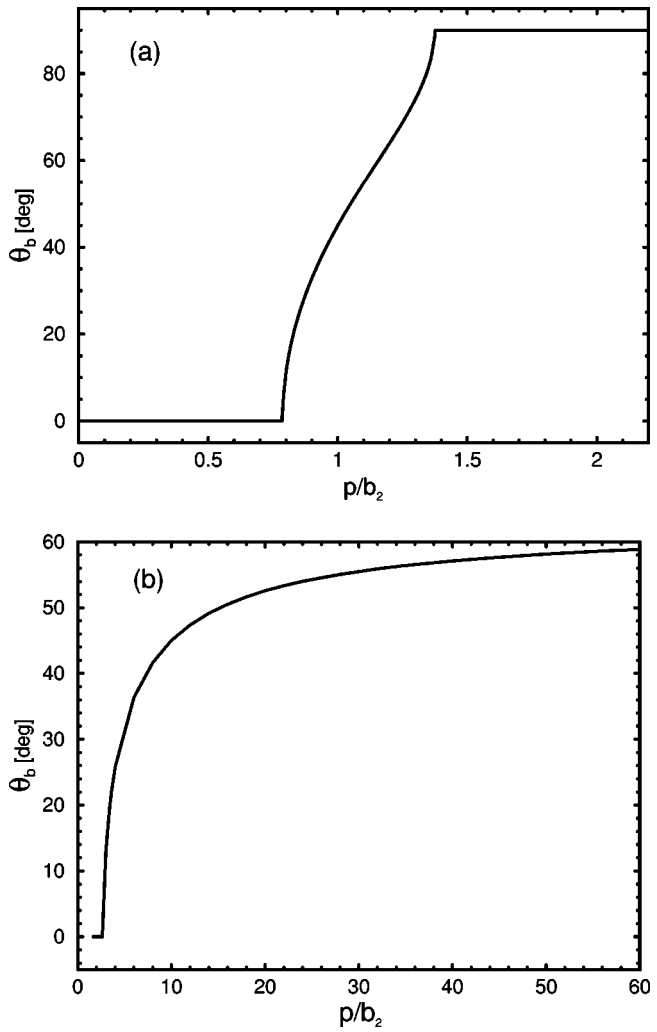

FIG. 4. Bulk value of the director orientation as a function of p/b_2 in the case of equal stripe widths ($p_1/p_2=1$), for (a) $p/b_1=1$ and (b) $p/b_1=10$.

the $(p/b_1, p/b_2)$ plane, for the two stripe width ratios $p_1/p_2=1$ [Fig. 3(a)] and $p_1/p_2=3$ [Fig. 3(b)]. The regions where the uniform configurations $\theta(x,z)=0$ and $\theta(x,z)=\pi/2$ are stable are called the U_0 phase and the $U_{\pi/2}$ phase, respectively. These uniform textures become unstable along the solid lines. In between, there is a region of stability of a nonuniform surface texture. Our calculations show that the phase transitions between the U_0 phase or the $U_{\pi/2}$ phase and the nonuniform texture (NT) are continuous. In Fig. 3(a), the phase diagram is symmetric with respect to the diagonal $p/b_1=p/b_2$. When the ratio $p_1/p_2>1$ the region of stability of the U_0 phase grows, whereas the region of stability of the $U_{\pi/2}$ phase shrinks [Fig. 3(b)]. Note that the phase diagram for $p_1/p_2<1$ can be easily deduced from the case $p_1/p_2>1$ by interchanging p_1 with p_2 and b_1 with b_2. The dashed lines in Fig. 3 correspond to the strong anchoring limit on one of the stripes discussed in the previous section.

In Figs. 4 and 5, we plot the bulk value of the director orientation $\theta_b=\theta(x,z=\infty)$ against p/b_2 at fixed p_1/p_2 and p/b_1. Even if the surface texture is not uniform the director field becomes uniform at infinite distance from the substrate. Thus, θ_b is independent of x and it corresponds to the effective anchoring direction induced by the inhomogeneous substrate. As we have already shown, θ_b is equal to the average of $\theta_0(x)$ over the period p [see Eq. (4.6)]. $\theta_b(p/b_2)$ for $p_1/p_2=1$ and $p/b_1=1$ is shown in Fig. 4(a). For this relatively small value of the anchoring strength on the homeotropic stripe, we observe two phase transtions between the uniform and nonuniform textures. In the NT region, θ_b increases from zero to $\pi/2$, starting and ending at transition lines with infinite slope. In Fig. 4(b), we present the case of $p_1/p_2=1$ and $p/b_1=10$. The latter value greatly exceeds the asymptotic value for the transition between the $U_{\pi/2}$ and NT phases. Thus, the curve $\theta_b(p/b_2)$ saturates at some value well below $\pi/2$. Similar plots are shown in Fig. 5(a) ($p/b_1=1$) and Fig. 5(b) ($p/b_1=10$), for the stripe width ratio $p_1/p_2=3$. Here again $p/b_1=1$ is below and $p/b_2=10$ is above the asymptotic value for the NT-$U_{\pi/2}$ transition.

The director orientation $\theta(x,z)$ as a function of x at fixed distance from the substrate is shown in Figs. 6 and 7. To

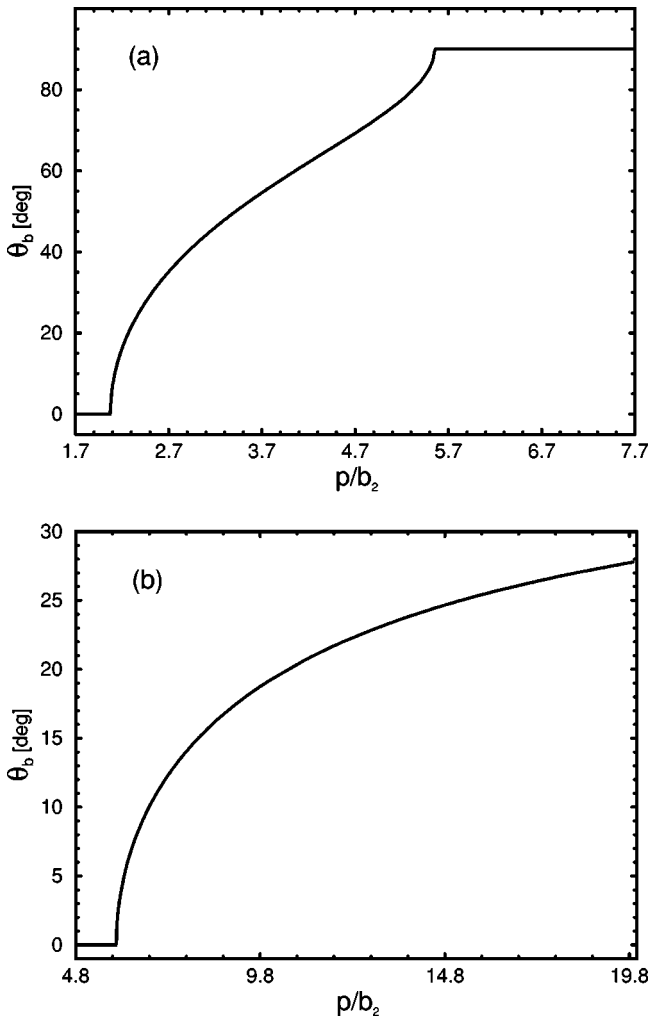

FIG. 5. Bulk value of the director orientation as a function of p/b_2 in the case of $p_1/p_2=3$, for (a) $p/b_1=1$ and (b) $p/b_1=10$.

obtain $\theta(x,z)$ from $\theta_0(x)$ we have used formula (4.3). It is clear from the Fourier expansion (3.2) that the decay of $\theta(x,z)-\theta_b$ for $z \gg p$ is governed by the $n=1$ term. Indeed, we observe that larger deviations of $\theta(x,z)$ from θ_b (horizontal line) occur only for $z<p$. Thus, the thickness of the surface layer is comparable to p. In all cases presented in Figs. 6 and 7 the choice of parameters corresponds to the NT phase. The case of equal stripe widths ($p_1/p_2=1$) is shown in Fig. 6. The profiles shown in Figs. 6(a) and 6(b) have been obtained for points in the $(p/b_1,p/b_2)$ plane close to the U_0-NT transition line; therefore, θ_b is small. While the profiles in Fig. 6(a) are roughly sinusoidal, in Fig. 6(b) they are highly asymmetric because in the latter case $p/b_1 \gg p/b_2$. Analogous behavior would be found for points near the NT-$U_{\pi/2}$ transition line, with θ_b close to $\pi/2$. For comparison, in Fig. 6(c), we show $\theta(x,z)$ for a point on the phase diagram located far from both transition lines. The case of different stripe widths is presented in Fig. 7, for $p_1/p_2=3$. Here, the asymmetry of the profiles reflects the difference in both the anchoring strength and the stripe width.

Finally, in Fig. 8, we compare the U_0-NT transition lines obtained from numerical minimization of the free energy and

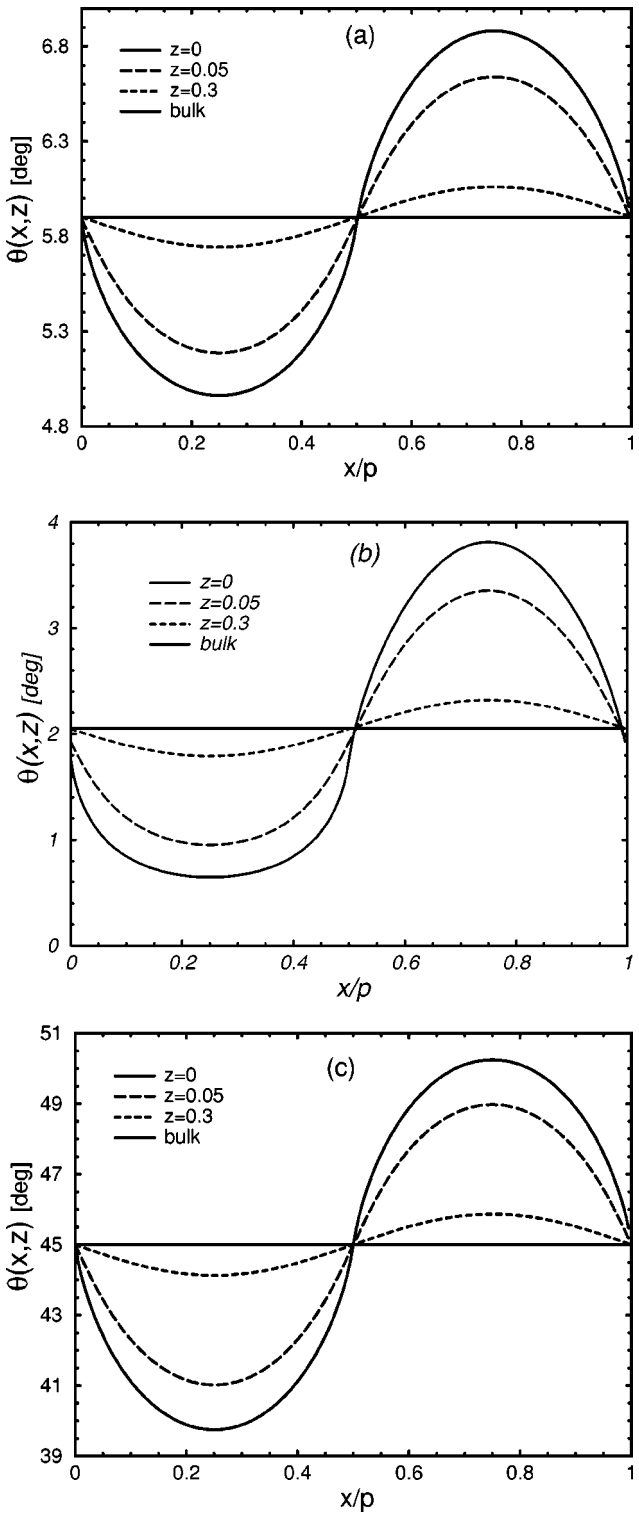

FIG. 6. Director orientation as a function of x, for a few values of the distance from the substrate. In this plot $p_1/p_2=1$, and (a) $p/b_1=1$, $p/b_2=0.79$, (b) $p/b_1=10$, $p/b_2=2.74$, (c) $p/b_1=1$, $p/b_2=1$.

from application of the square gradient approximation, for $p_1/p_2=1$ and $p_1/p_2=3$. Of course, using the same approximation we can also find an approximate location of the NT-$U_{\pi/2}$ transition line, which is not shown in Fig. 8, how-

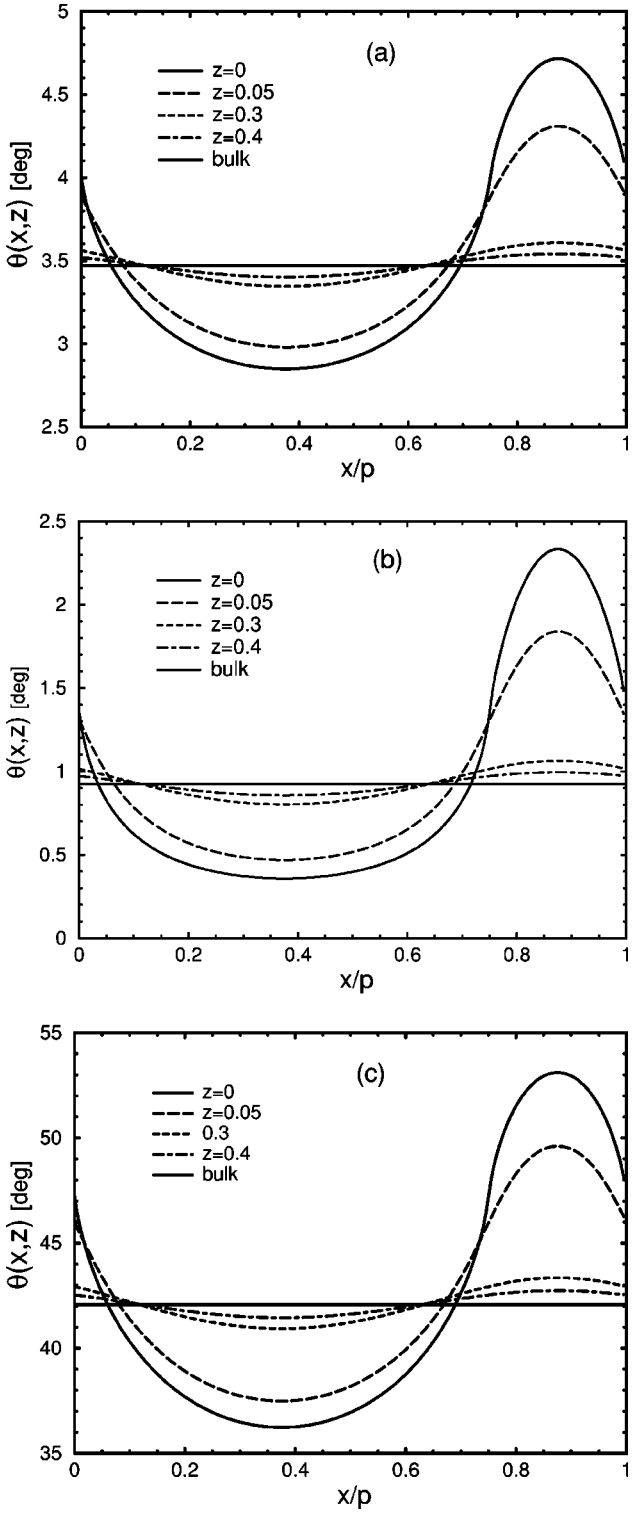

FIG. 7. Director orientation as a function of x, for a few values of the distance from the substrate. In this plot $p_1/p_2=3$, and (a) $p/b_1=1$, $p/b_2=2.08$, (b) $p/b_1=6.5$, $p/b_2=5.24$, (c) $p/b_1=1$, $p/b_2=3$.

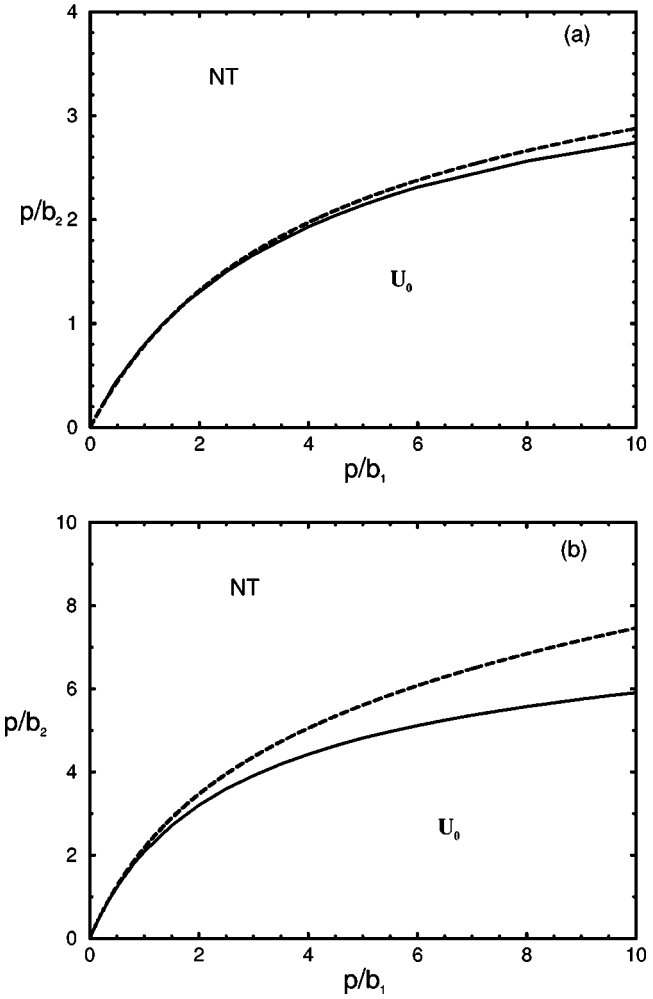

FIG. 8. Comparison of the U_0-NT transition lines obtained from the square gradient approximation (dashed line) and from numerical minimization of the free energy functional (solid line): (a) $p_1/p_2=1$ and (b) $p_1/p_2=3$. For clarity, the NT-$U_{\pi/2}$ transition line is not shown.

ever. It is clear that the square gradient approximation becomes increasingly accurate when the anchoring strengths decrease, whereas in the opposite limit we observe larger deviations from the real transition line.

V. CONCLUSIONS

We have studied the nematic phase in contact with a solid substrate of periodic surface structure using the Frank-Oseen description of the liquid crystal. The reason for using the description of the system in terms of $\hat{\mathbf{n}}$ rather than in terms of the tensor $\mathbf{Q}$ (the Landau–de Gennes description) is that the extrapolation length, which is a natural length scale in surface problems, is much more easily accessible in the former than in the latter. We have assumed that the substrate surface consists of regions of competing alignments: homeotropic on one of the stripes and planar along the normal to the stripes on the other. This competition may result in either a uniform or a nonuniform texture. The latter is favored when the stripes have comparable widths and anchoring strengths. When the anchoring strength on one of the stripes is much larger than on the other, the regions with stronger anchoring may enforce an unfavorable alignment in regions with weaker anchoring, which results in a uniform texture. This

resembles the situation when a nematic slab is placed in an external field normal to the alignment favored by the walls and the field is too weak to perturb this alignment.

We have also considered the limit of strong anchoring on one of the stripes and weak anchoring on the other. An interesting bifurcation problem arises when the width p_1 of the strong anchoring stripe tends to zero. Now the question is about the minimal value of the anchoring energy w_{min} in the weak anchoring regions necessary to perturb the alignment induced by the strong anchoring regions. Intuitively it might appear that this minimal value should also tend to zero. On the other hand, any continuous perturbation of the initial uniform alignment should satisfy suitable boundary conditions along the borderlines between the regions of strong and weak anchoring. The usual procedure of taking the Fourier transform of the perturbation and truncating the Fourier series at a finite number N leads to the conclusion that $w_{min}(N) \neq 0$. However, when the number of Fourier components increases $w_{min}(N)$ decreases and the whole procedure does not lead to any definite conclusion. Moreover, our results suggest that the order of taking the limits $N \to \infty$ and $p_1 \to 0$ does matter in this case. Probably we observe the following situation. The perturbation corresponding to the true w_{min} tends to a constant profile when $p_1 \to 0$, which means that the strong anchoring regions transform into disclination lines. To obtain the correct asymptotic behavior of $w_{min}(p_1)$ for $p_1 \to 0$ as well as the functional form of the corresponding perturbation, a more subtle bifurcation analysis is needed, and studies of this problem are in progress.

ACKNOWLEDGMENT

This work was supported in part by the KBN Grant No. 5P03B01121.

[1] P.G. de Gennes and J. Prost, *The Physics of Liquid Crystals*, 2nd ed. (Clarendon, Oxford, 1993).
[2] B. Jérôme, Rep. Prog. Phys. **54**, 391 (1991).
[3] J. Cognard, Mol. Cryst. Liq. Cryst. Suppl. Ser. **1**, 1 (1982).
[4] J.M. Geary, J.W. Goodby, A.R. Kmetz, and J.S. Patel, J. Appl. Phys. **62**, 4100 (1987).
[5] J.L. Janning, Appl. Phys. Lett. **21**, 173 (1972).
[6] V.K. Gupta and N.L. Abbot, Science **276**, 1533 (1997).
[7] L. Komitov, G.P. Bryan-Brown, E.L. Wood, and A.B.J. Smout, J. Appl. Phys. **86**, 3508 (1999).
[8] T.J. Sluckin and A. Poniewierski, in *Fluid Interfacial Phenomena*, edited by C.A. Croxton (J. Wiley, Chichester, 1986).
[9] A.K. Sen and D.E. Sullivan, Phys. Rev. A **35**, 1391 (1987).
[10] P.I.C. Teixeira, T.J. Sluckin, and D.E. Sullivan, Liq. Cryst. **14**, 1243 (1993).
[11] B. Jérôme and P. Pieranski, J. Phys. (France) **49**, 1601 (1988).
[12] A. Poniewierski and A. Samborski, Liq. Cryst. **27**, 1285 (2000).
[13] D.W. Berreman, Phys. Rev. Lett. **28**, 1683 (1972).
[14] S. Faetti, Phys. Rev. A **36**, 408 (1987).
[15] G. Barbero, T. Beica, A.L. Alexe-Ionescu, and R. Moldovan, J. Phys. II **2**, 2011 (1992).
[16] T.Z. Qian and P. Sheng, Phys. Rev. Lett. **77**, 4564 (1996).
[17] T.Z. Qian and P. Sheng, Phys. Rev. E **55**, 7111 (1997).
[18] Baek-woon Lee and N.A. Clark, Science **291**, 2576 (2001).
[19] A. Rapini and M. Papoular, J. Phys. (Paris), Colloq. **30**, C4-54 (1969).
[20] P. Pieranski, F. Brochard, and E. Guyon, J. Phys. (France) **33**, 681 (1972).
[21] J. Wahl and F. Fisher, Mol. Cryst. Liq. Cryst. **22**, 359 (1973).
[22] W.H. Press, B.P. Flannery, S.A. Teukolsky, and W.T. Vetterling, *Numerical Recipes* (Cambridge University Press, Cambridge, 1986).